*Int. J. Heat Mass Transfer.* Vol. 31, No. 4, pp. 743–757, 1988
Printed in Great Britain

0017–9310/88 $3.00 + 0.00


# Transient response of a steady vertical flow subject to a change in surface heating rate

YOGENDRA JOSHI
Department of Mechanical Engineering, Naval Postgraduate School, Monterey, CA 93943, U.S.A.

and

BENJAMIN GEBHART
Department of Mechanical Engineering and Applied Mechanics University of Pennsylvania, Philadelphia, PA 19104, U.S.A.

(*Received* 17 *February* 1987 *and in final form* 12 *August* 1987)

**Abstract**—Transient natural convection response, following a change in heating rate at a surface, has been measured over a range of heating conditions, in water. A new steady state is achieved through several distinct processes. The first is a superimposed purely diffusive transient near the surface, which agrees with the solutions given. The flow then diverges into a general downstream developing transient. Flow solutions then indicate a propagating leading edge effect downstream. Thereafter, the transient approaches a new steady flow. Transport response, determined by visualizations and local velocity and temperature measurements, also agree with the calculations. Upstream flows remain laminar throughout the transient. Downstream, both transient transition and turbulence enhance local heat transfer. This suggests that general heat transfer enhancement may be achieved by programmed changes in imposed heat flux levels.

## 1. INTRODUCTION

TRANSIENT vertical natural convection flow response, following from a suddenly imposed surface heating condition, has been studied in considerable detail. Following the early work of Illingworth [1], the sequence of events resulting in the final two-dimensional laminar boundary layer flow has been studied both in experiments and analysis, as summarized in ref. [2]. At the beginning of a transient, the flow adjacent to a vertical surface with a leading edge is one-dimensional. The presence of the leading edge is successively felt downstream, as ambient entrainment develops a two-dimensional field. The flow then eventually becomes steady boundary region transport. The sequence of events in very vigorous flows, which undergo transition, is reported in ref. [3].

In many technological and environmental applications, transients are actually caused, not by imposed temperature changes, but by a changing level of an existing energy input. Many such transients do not start from quiescence, but from a previous heating and resulting flow condition. An example is a solar collector panel, when solar insolation suddenly changes, possibly due to changing cloud cover. An initial steady flow becomes a transient which ultimately may result in another steady flow condition.

Ingham [4] considered such a transient, that following a sudden disappearance of the previous heating condition along a vertical isothermal surface. The initial steady flow was taken as that generated by a surface at temperature $t_0$, in a quiescent ambient at $t_\infty$. The surface temperature was then changed to $t_\infty$. The resulting decaying transient flow was calculated for short and for long times. The short-time analysis applies as long as the effect of the change is felt only very close to the surface. Then, only the effects of thermal diffusion near the surface are important. This amounts to a one-dimensional transient effect in the flow. For such impulsive temperature conditions, the generalized coordinate normal to the surface is $\xi = y/2(v\bar{\tau})^{1/2}$. The governing equations describing the decaying flow are recast in terms of $\xi$ and $\tau = \bar{\tau}/\sqrt{x}$, where $x$ is the distance from the leading edge. A series solution was obtained in terms of $\tau$, valid for $\tau \ll 1$.

The approach to steady state, for $\tau \gg 1$, is the gradual disappearance of all flow. This was calculated as an expansion, by balancing the dominant terms in the governing equations. Only the leading order solutions were given. The higher order terms involve eigenfunctions, due to the uncertainty associated with conditions at $\tau = 0$. The numerical solution for this transient [4] matches the small and large time solutions well. Similar results were given by Ingham *et al.* [5], for the sudden temperature change of a vertical surface imbedded in a porous medium.

The condition of a sudden increase or decrease in temperature is convenient for analysis. However, such changes are seldom, if ever, realized. The condition that often better approximates reality is a sudden change in an energy input or generation rate in the surface material. As part of an investigation of a suddenly initiated heat condition, Sammakia *et al.* [6]

## NOMENCLATURE

| | |
|---|---|
| $c''$ | surface thermal capacity per unit area |
| $c_p$ | specific heat |
| $E$ | beginning of transition parameter, $G^*(v^2/gx^3)^{2/15}$ |
| $f$ | non-dimensional stream function, $\psi/(U_c\delta)$ |
| $g$ | acceleration due to gravity |
| $G^*$ | modified flux Grashof number, $5(Gr_x^*/5)^{1/5}$ |
| $Gr_x^*$ | local flux Grashof number, $g\beta q_1'' x^4/kv^2$ |
| $k$ | thermal conductivity of fluid |
| $Pr$ | fluid Prandtl number |
| $Q^*$ | thermal capacity parameter defined in equation (26) |
| $q_1''$ | initial surface heat flux |
| $q_2''$ | final surface heat flux |
| $t$ | temperature (dimensional) |
| $T$ | temperature (nondimensional) |
| $u$ | vertical velocity (dimensional) |
| $U$ | vertical velocity (nondimensional) |
| $U_c$ | characteristic velocity, $vG^*/5x$ |
| $v$ | horizontal velocity (dimensional) |
| $V$ | horizontal velocity (nondimensional) |
| $W$ | thickness of the surface element |
| $x$ | vertical coordinate (dimensional) |
| $X$ | vertical coordinate (nondimensional) |
| $y$ | horizontal coordinate (dimensional) |
| $Y$ | horizontal coordinate (nondimensional). |

Greek symbols

| | |
|---|---|
| $\alpha$ | thermal diffusivity of fluid |
| $\beta$ | coefficient of thermal expansion of fluid |
| $\delta$ | initial boundary layer thickness, $5x/G^*$ |
| $\eta$ | non-dimensional distance coordinate, $y/\delta$ |
| $\nu$ | kinematic viscosity of fluid |
| $\xi$ | non-dimensional distance, $y/2(v\bar{\tau})^{1/2}$ |
| $\rho$ | density |
| $\tau$ | non-dimensional time |
| $\bar{\tau}$ | dimensional time |
| $\phi$ | non-dimensional temperature coordinate |
| $\psi$ | stream function. |

Subscripts

| | |
|---|---|
| 0 | value at the surface |
| 1 | quantity based on $q_1''$ |
| 2 | quantity based on $q_2''$ |
| $\infty$ | value in the ambient |
| BL | laminar boundary layer |
| FD | finite difference calculation |
| f | fluid |
| s | surface. |

also considered transport following a cessation of surface heating. Finite difference transport solutions were obtained. Comparisons indicated that computations and measurements of surface temperature response, were in good agreement. However, as there were no flow visualizations or sensor measurements in the fluid, it is difficult to surmise the transient behavior of various flow features, including entrainment and any disturbance effects which arose.

Our investigation examined the general transient natural convection response arising from a sudden change of the level of energy input flux to a vertical surface element. That is, a steady input heat flux $q_1''$ is changed, at $\tau = 0$, to a new steady level $q_2''$, for $\tau > 0$. The short-time analysis, given in Section 2, is similar to that given by Ingham [4]. However, the actual generalizations and transformed equations are different, since the surface flux condition was taken. Closed form solutions are found, for surface elements having a relatively negligible thermal capacity, compared to the adjacent fluid. This was water in the experiments.

These short-time solutions are compared to the numerical transient finite difference calculations, using the complete transient boundary layer equations in Section 3. Explicit time integration with a spatially variable grid size was used. Since this numerical formulation is not limited to short times, the calculations were continued to steady state. These numerical and analytical solutions were also verified by experiments, in water, in terms of local sensor data and flow visualizations. In Section 4, the experimental data are compared with both the short-time analysis and the numerical results. The flow visualizations, and their implications concerning flow response, are then considered.

## 2. SHORT-TIME TRANSIENT RESPONSE

The initial steady transport is a two-dimensional natural convection boundary region flow in a quiescent fluid at $t_\infty$, with a uniform flux dissipation rate at the surface $q_1''$. A transient begins when this flux is changed to $q_2''$, for $\tau \geqslant 0$. With the Boussinesq approximations, the equations for the transient response are

$$\frac{\partial u}{\partial x} + \frac{\partial v}{\partial y} = 0 \tag{1}$$

$$\frac{\partial u}{\partial \bar{\tau}} + u\frac{\partial u}{\partial x} + v\frac{\partial u}{\partial y} = g\beta(t - t_\infty) + \nu\frac{\partial^2 u}{\partial y^2} \tag{2}$$

$$\frac{\partial t}{\partial \bar{\tau}} + u\frac{\partial t}{\partial x} + v\frac{\partial t}{\partial y} = \alpha\frac{\partial^2 t}{\partial y^2}. \tag{3}$$

For time $\bar{\tau} \leqslant 0$, the steady flow resulted from the uniform surface flux $q_1''$. For $\bar{\tau} > 0$, the flux is $q_2''$. The

thermal capacity of the surface element is assumed to be negligible, compared to that of the fluid. This is often a very good approximation for thin surfaces in liquids, as shown by the calculations in the Appendix. For $\bar{\tau} \geqslant 0$, the time-dependent stream and temperature functions $f$ and $\phi$ are formulated as

$$\psi = U_e(x)\delta(x)f(\eta, t); \quad u = \partial\psi/\partial y; \quad v = -\partial\psi/\partial x \tag{4a}$$

$$\phi(\eta, \tau) = \frac{(t - t_\infty)}{\Delta T}, \quad \Delta T = q_1''\delta(x)/k \tag{4b}$$

where $\eta = y/\delta(x)$, $\delta(x) = 5x/G^*$, $U_e(x) = \nu G^{*2}/5x$, $\tau = \nu\bar{\tau}/[\delta(x)]^2$ and

$$G^* = 5(Gr_x^*/5)^{1/5} \quad \text{and} \quad Gr_x^* = \frac{g\beta q_1'' x^4}{k\nu^2}. \tag{5}$$

In equations (4) and (5), $U_e(x)$ is the characteristic velocity, $\delta(x)$ is the boundary layer thickness at $\tau = 0$ and $Gr_x^*$ is the local flux Grashof number based on the initial heat flux, $q_1''$.

Introducing equations (4) and (5) into equations (1)–(3) reduces the independent variables from $x$, $y$ and $\bar{\tau}$ to $\eta$ and $\tau$. The transformed equations in $f(\eta, \tau)$ and $\phi(\eta, \tau)$ are

$$\frac{\partial^3 f}{\partial\eta^3} + \phi + \frac{\partial^2 f}{\partial\eta\,\partial\tau}\left[-1 + 2\tau\frac{\partial f}{\partial\eta}\right] + \frac{\partial^2 f}{\partial\eta^2}\left[4f - 2\tau\frac{\partial f}{\partial\tau}\right] - 3\left(\frac{\partial f}{\partial\eta}\right)^2 = 0 \tag{6}$$

$$\frac{\partial^2\phi}{\partial\eta^2} + Pr\frac{\partial\phi}{\partial\tau}\left[-1 + 2\tau\frac{\partial f}{\partial\eta}\right] + Pr\frac{\partial\phi}{\partial\eta}\left[4f - 2\tau\frac{\partial f}{\partial\tau}\right] - Pr\,\phi\frac{\partial f}{\partial\eta} = 0. \tag{7}$$

The boundary conditions, for $\tau \geqslant 0$, are

$$\frac{\partial\phi}{\partial\eta}(0, \tau) = -(q_2''/q_1''); \quad \frac{\partial f}{\partial\eta}(0, \tau) = f(0, \tau) = 0 \tag{8a}$$

$$\phi(\infty, \tau) = \frac{\partial f}{\partial\eta}(\infty, \tau) = 0 \tag{8b}$$

where equation (8a) applies at the surface. Equation (8b) applies in the ambient medium, assumed to remain unstratified and quiescent. The transport at $\tau = 0$ is a steady downstream developing flow, $f_0(\eta) = f(\eta, 0)$ and $\phi_0(\eta) = \phi(\eta, 0)$, where $f_0(\eta)$ and $\phi_0(\eta)$ are solutions of

$$f_0''' + \phi_0 + 4f_0 f_0'' - 3f_0'^2 = 0 \tag{9}$$

$$\phi_0'' + 4Pr\, f_0\phi_0' - Pr\,\phi_0 f_0' = 0 \tag{10}$$

where

$$f_0(0) = f_0'(0) = 1 + \phi_0'(0) = \phi_0(\infty) = f_0'(\infty) = 0. \tag{11}$$

Equations (9) and (10) follow from equations (6) and (7) when time derivatives are taken as zero.

### 2.1. *Series solution for short times*

Equations (6)–(8) are next re-written in a form more convenient for analysis at short times. In all impulsive changes at a surface, there is a brief period in which the effects are confined to a thin, one-dimensional layer adjacent to the surface. Specifically, for $\nu\bar{\tau}/\delta^2 = \tau \ll 1$, there exists an 'inner layer' which is described by equations (6)–(8). Outside this layer, the flow remains the initial boundary layer profile, as given by $f_0$ and $\phi_0$ in equations (9) and (10). Since the appropriate length for short times is the diffusion scale $(\tau)^{1/2}$, the normalized distance scale is then $\xi = \eta/(2\tau)^{1/2} = y/2(\nu\bar{\tau})^{1/2}$. Therefore, the $f$ and $\phi$, in equations (4), are further transformed as

$$f(\eta, \tau) = \tau^2 F(\xi, \tau); \quad \phi(\eta, \tau) = \tau^{1/2}\theta(\xi, \tau). \tag{12}$$

Introducing this into equations (6) and (7) yields

$$\frac{1}{8}\frac{\partial^3 F}{\partial\xi^3} + \theta - \frac{3}{4}\frac{\partial F}{\partial\xi} + \frac{\partial^2 F}{\partial\xi\,\partial\tau}\left[-\frac{\tau}{2} + \frac{\tau^{7/2}}{2}\frac{\partial F}{\partial\xi}\right] = 0 \tag{13a}$$

$$\frac{1}{4}\frac{\partial^2\theta}{\partial\xi^2} - Pr\frac{\partial\theta}{\partial\tau}\left[\tau\left(1 - \tau^{5/2}\frac{\partial F}{\partial\xi}\right)\right] - Pr\frac{\theta}{2} + Pr\frac{\partial\theta}{\partial\xi}\left[\frac{\xi}{2} - \tau^{7/2}\frac{\partial F}{\partial\tau}\right] = 0. \tag{13b}$$

The boundary conditions at $\xi = 0$ ($y = 0$) are

$$F(0, \tau) = \frac{\partial F}{\partial\xi}(0, \tau) = 0; \quad \frac{\partial\theta}{\partial\xi}(0, \tau) = -2(q_2''/q_1'').$$

The solutions in this growing 'inner' layer are taken to match the outer steady boundary layer. This is approximated at small $\eta$ as

$$f_0 \sim a\eta^2/2 - b\eta^3/6 + \eta^4/24 + a^2\eta^5/60 + O(\eta^6) \tag{14a}$$

$$\phi_0 \sim b - n + O(\eta^3). \tag{14b}$$

Both $a = f_0''(0)$ and $b = \phi_0(0)$ depend on $Pr$. Substitution of equations (12) into equations (14) yields, for large $\xi$

$$F(\xi, \tau) \sim 2\xi^2 a/\tau - 4b\xi^3/3\tau^{1/2} + 2\xi^4/3 + 8a^2\xi^5\tau^{1/2}/15 + O(\tau) \tag{15a}$$

$$\phi(\xi, \tau) \sim b\tau^{-1/2} - 2\xi + O(\tau). \tag{15b}$$

The behavior of the inner layer as $\xi \to \infty$ is to be matched with the outer solution, $f_0$, $\phi_0$. Equations (15) suggest solutions of the following form:

$$F(\xi, \tau) = \tau^{-1}F_0(\xi) + \tau^{-1/2}F_1(\xi) + F_2(\xi) + \tau^{1/2}F_3(\xi) + O(\tau) \tag{16a}$$

$$\theta(\xi, \tau) = \tau^{-1/2}H_0(\xi) + H_1(\xi) + O(\tau). \tag{16b}$$

These are substituted into equations (13). Terms with equal powers of $\tau$ are collected to obtain

$$F_0''' - 2F_0'' + 2\xi F_0'' = 0 \quad (17a)$$

$$F_1''' - 4F_1' + 2\xi F_1'' + 8H_0 = 0 \quad (17b)$$

$$F_2''' - 6F_2' + 2\xi F_2'' + 8H_1 = 0 \quad (17c)$$

$$F_3''' - 8F_3' + 2\xi F_3'' + 4F_0F_0'' - 4F_0'^2 = 0 \quad (17d)$$

$$H_0'' + 2Pr\,\xi H_0' = 0 \quad (17e)$$

$$H_1'' + 2Pr\,\xi H_1' - 2Pr\,H_1 = 0. \quad (17f)$$

The boundary conditions are: for $i = 1$–$3$;

$$F_i'(0) = F_i(0) = 0; \quad H_0'(0) = 0;$$

$$H_1'(0) = -2(q_2''/q_1'') \quad (18a)$$

$$\text{as } \xi \to \infty; \quad F_0(\xi) \sim 2a\xi^2; \quad F_1(\xi) \sim -\tfrac{4}{3}b\xi^3 \quad (18b)$$

$$F_2(\xi) \sim \tfrac{2}{3}\xi^4; \quad F_3(\xi) \sim \tfrac{8}{15}a^2\xi^5 \quad (18c)$$

$$H_0(\xi) \sim b; \quad H_1(\xi) \sim -2\xi. \quad (18d)$$

2.1.1. *The response for the inner layer.* Solutions for $F_0$, $F_1$, $F_2$, $F_3$, $H_0$ and $H_1$, with the boundary conditions in equations (18), have been obtained in closed form. The resulting expressions for $H(\xi, \tau)$ and $\partial F/\partial\xi(\xi, \tau)$ are then calculated using equations (16). These are

$$\theta = b\tau^{-1/2} + 2(q_2''/q_1'' - 1) \times [e^{-\xi^2 Pr} - \xi\sqrt{Pr}\,\pi\,\text{erfc}\,(\xi\sqrt{Pr})]/\sqrt{\pi\,Pr} \quad (19)$$

for $Pr \neq 1$

$$\frac{\partial F}{\partial\xi} = 4a\xi\tau^{-1} - 4b\xi^2\tau^{-1/2} + 16(1 - q_2''/q_1'') \times [\text{i}^3\,\text{erfc}\,\xi - \text{i}^3\,\text{erfc}\,(\xi\sqrt{Pr})]/\{(1-Pr)\sqrt{Pr}\} + 8\xi^3/3 + 8a^2\xi^4\tau^{1/2}/3 + O(\tau) \quad (20)$$

for $Pr = 1$

$$\frac{\partial F}{\partial\xi} = 4a\xi\tau^{-1} - 4b\xi^2\tau^{-1/2} - 8\xi(1 - q_2''/q_1'') \times \text{i}^2\,\text{erfc}\,\xi + 8\xi^3/3 + 8a^2\xi^4\tau^{1/2}/3 + O(\tau) \quad (21)$$

where the integrals of the error function in equations (20) and (21) are defined as

$$\text{i}^n\,\text{erfc}\,x = \int_x^\infty \text{i}^{n-1}\,\text{erfc}\,y\,dy \text{ for } n \geqslant 1$$

$$\text{and} \quad \text{i}^0\,\text{erfc}\,x = \text{erfc}\,x.$$

2.1.2. *Composite solutions valid for all $\eta$.* Equations (19)–(21) apply to the inner layer, that is for $\eta \ll 1$. Short-time solutions valid for all $\eta$ are obtained by first writing equations (19)–(21) in terms of $\eta$ and subsequently combining them with the outer solutions $d(f_0(\eta))/d\eta$ and $\phi_0(\eta)$. The resulting velocity and temperature function $f'(\eta, \tau)$ and $\phi(\eta, \tau)$ are

for $Pr \neq 1$

$$\frac{\partial f}{\partial\eta} = \frac{df_0(\eta)}{d\eta} + \frac{8\tau^{3/2}(1 - q_2''/q_1'')}{(1-Pr)\sqrt{Pr}} \times \left[\text{i}^3\,\text{erfc}\left[\frac{\eta}{2\sqrt{\tau}}\right] - \text{i}^3\,\text{erfc}\left[\frac{n\sqrt{Pr}}{2\sqrt{\tau}}\right]\right] \quad (22a)$$

for $Pr = 1$

$$\frac{\partial f}{\partial\eta} = \frac{df_0(\eta)}{d\eta} - 4\eta\tau^{3/2}(1 - q_2''/q_1'') \times \text{i}^2\,\text{erfc}\,(\eta/2\sqrt{\tau}) + O(\tau^{5/2}) \quad (22b)$$

and

$$\phi = \phi_0(\eta) + \frac{2\tau^{1/2}}{\sqrt{Pr}}(q_2''/q_1'' - 1) \times \text{i}\,\text{erfc}\left[\frac{\eta}{2}\frac{\sqrt{Pr}}{\sqrt{\tau}}\right] + O(\tau^{3/2}). \quad (22c)$$

Equations (22a) and (22c) are plotted in Figs. 1 and 2, for water, $Pr = 6.2$, and in Figs. 3 and 4 for air, $Pr = 0.7$. Values for $q_2''/q_1'' = 5$ and 0.5 were chosen. Comparing Figs. 1 and 2 with Figs. 3 and 4 shows that, for both heating conditions, transient response in air is faster, in terms of $\tau$. This is also true in physical time $\bar{\tau}$. In water, the larger density and viscous forces retard changes in fluid velocity. An important quantity is the shear stress at the surface. This is

$$\left.\frac{\partial^2 f}{\partial\eta^2}\right|_{\eta=0} = \left.\frac{d^2 f_0}{d\eta^2}\right|_{\eta=0} + \frac{4\tau(1 - q_2''/q_1'')}{(1-Pr)\sqrt{Pr}} \times (\sqrt{Pr} - 1)\,\text{i}^2\,\text{erfc}\,(0). \quad (23)$$

Surface shear stress development with time is shown in Fig. 5, over a range of $q_2''/q_1''$, for both water and air. An increase in surface heat flux increases surface shear. The change of surface shear, $f''(0, \tau)$, for a given value of $q_2''/q_1''$, is larger in air.

## 3. NUMERICAL SIMULATION OF THE ENTIRE TRANSIENT RESPONSE

The short-time solutions given in Section 2 apply while transient effects are confined to the fluid region very near the surface, well within the initial thermal boundary layer. These effects continue to penetrate outward and eventually cause a new steady flow. Numerical solutions of equations (1)–(3) were therefore determined, for the whole transient, assumed to be laminar, from $\tau = 0$ to the eventual steady state. The results given here are for water, $Pr = 6.2$.

Equations (1)–(3) were nondimensionalized in a manner similar to that of Sammakia *et al.* [6], using the initial heat flux $q_1''$. A completely equivalent formulation is also obtained using $q_2''$. The new variables are

$$X, Y = x, y/(v^2k/g\beta q_1'')^{1/4} \quad (24a)$$

$$U, V = u, v/(v^2 g\beta q_1''/k)^{1/4} \quad (24b)$$

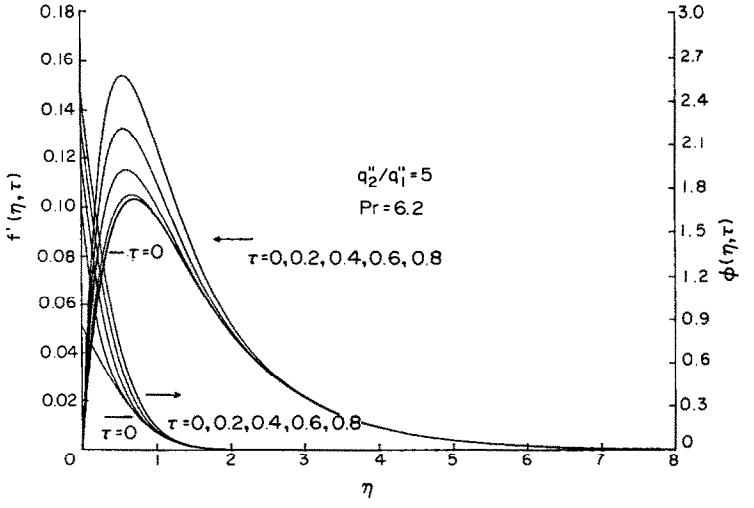


FIG. 1. Short-time velocity and temperature responses across the boundary region following an increase in surface heating for $q_2''/q_1'' = 5$ and $Pr = 6.2$.

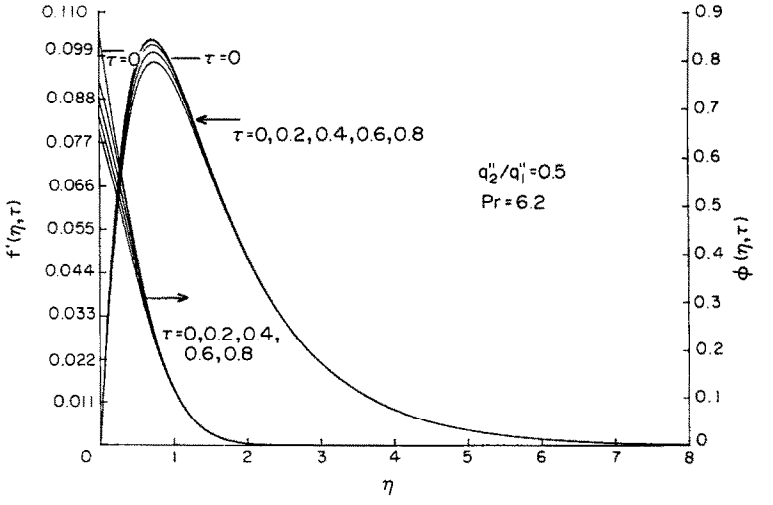


FIG. 2. Short-time velocity and temperature responses across the boundary region following a decrease in surface heating for $q_2''/q_1'' = 0.5$ and $Pr = 6.2$.

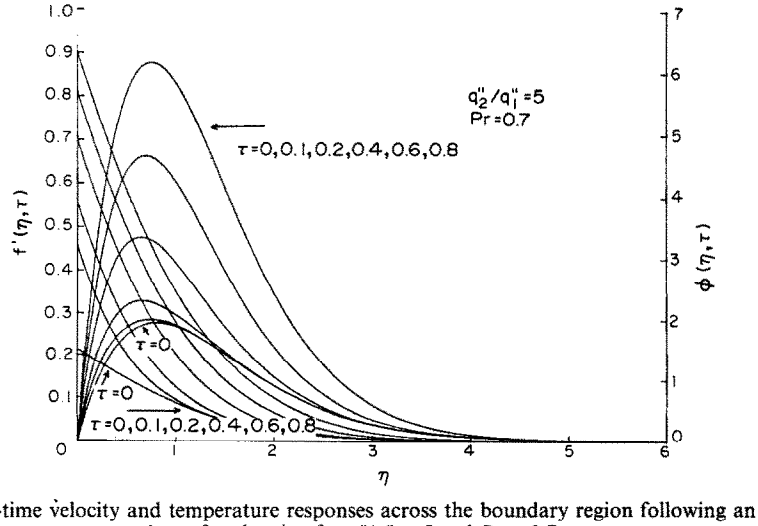


FIG. 3. Short-time velocity and temperature responses across the boundary region following an increase in surface heating for $q_2''/q_1'' = 5$ and $Pr = 0.7$.

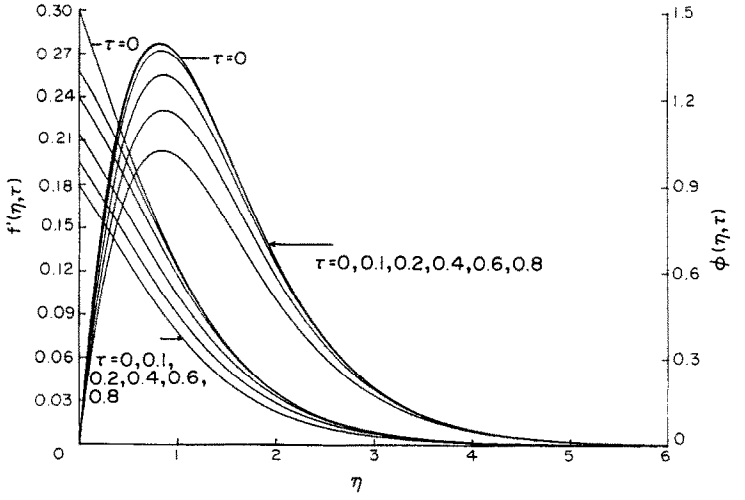


FIG. 4. Short-time velocity and temperature responses across the boundary region following a decrease in surface heating for $q_2''/q_1'' = 0.5$ and $Pr = 0.7$.

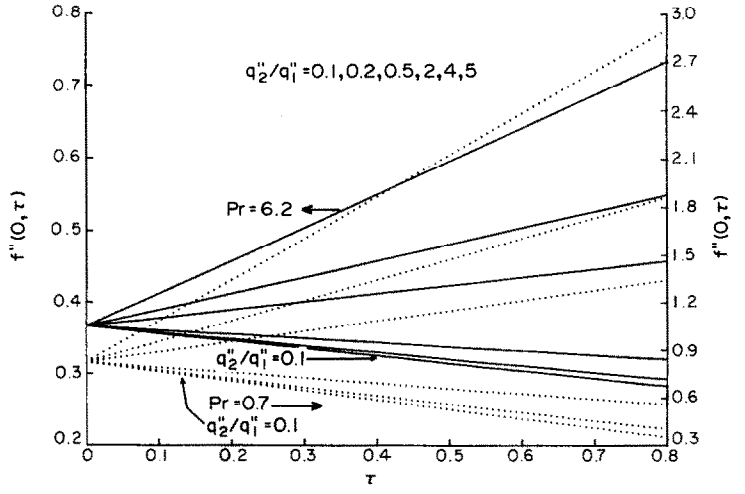


FIG. 5. Non-dimensional surface shear variation for short times for various $q_2''/q_1''$: ———, $Pr = 6.2$; · · · · · · · , $Pr = 0.7$.

$$T = (t - t_\infty)/(\nu^2 q_1''^3/g\beta k^3)^{1/4} \quad (24c)$$

$$\tau_{FD} = \bar{\tau}(k/g\beta q_1'')^{1/2}. \quad (24d)$$

In equation (24d), the subscript FD refers to the finite difference calculation. The initial and boundary conditions are

$$\text{at} \quad \tau_{FD} = 0; \quad U = U_1, \quad V = V_1 \quad \text{and} \quad T = T_1 \quad (25a)$$

$$\text{at} \quad X = 0; \quad U = V = T = 0 \quad (25b)$$

$$\text{at} \quad Y = 0; \quad U = V = 0 \quad (25c)$$

and also

$$\text{at} \quad Y = 0; \quad q_2''/q_1'' = Q^* \partial T/\partial \tau_{FD} - \partial T/\partial Y. \quad (25d)$$

The surface thermal capacity effect was included in these calculations. The last condition, equation (25d), is the resulting energy balance at the surface. The parameter $Q^*$ represents thermal energy storage capacity of the surface element. For an element the thermal capacity per unit surface area of which is $c''$, $Q^*$ is given by

$$Q^* = c''[g\beta q_1'' \nu^2/k^5]^{1/4}. \quad (26)$$

Numerical calculations using the above formulation, with $Q^* = 0$, were in agreement with the short-time solutions in Section 2. Continuing calculations then determined the transient development to the new steady state at $q_2''$. These calculations are discussed next. Also included are the effects of surface element thermal capacity, that is $Q^* \neq 0$. In Section 4, these results are compared with the experimental data, in water at room temperature.

### 3.1. *Numerical solution scheme*

An explicit finite difference scheme described in Carnahan *et al.* [7] and also employed by Sammakia

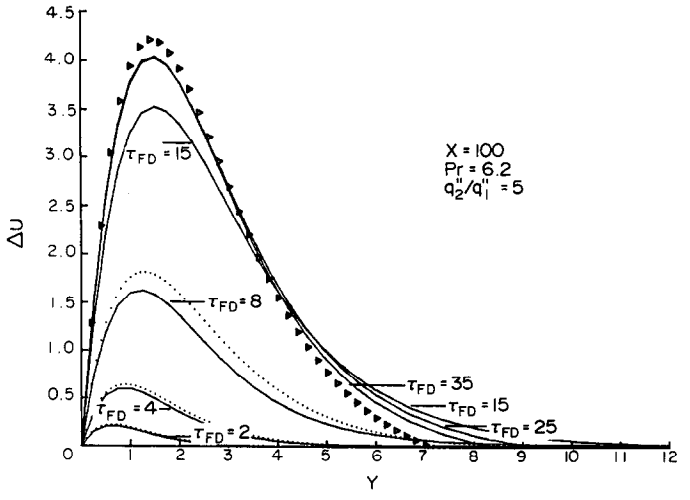


FIG. 6. Incremental vertical velocity profiles across the fluid at various times for $q''_2/q''_1 = 5$ and $Pr = 6.2$: ———, finite-difference calculations; · · · · · · ·, short-time analysis; ▷, steady laminar similarity solution.

*et al.* [6] was used for all calculations reported here. Initial steady-state profiles were first obtained from equations (9)–(11). The starting values $U_1$, $V_1$ and $T_1$ at each grid point were then interpolated from the known $f'_0(\eta)$ and $\phi_0(\eta)$, using cubic spline polynomials. A variable grid was employed in both the $X$- and $Y$-directions. This enabled the deployment of a larger number of grid points near both $X = 0$ and $Y = 0$, where the largest gradients occur.

A $40 \times 40$ grid was used and $X_{max} = 100$ and $Y_{max} = 25$ were taken for comparison with the short-time solutions. These correspond to $Gr^*_L = 10^8$ and $\eta_{max} = 7.21$, where $Gr^*_L$ is the Grashof number at the top of the surface and $\eta_{max}$ is the extent of the transport region in the non-dimensional coordinates in equations (5). The numerical scheme results in an upper limit on the allowable time step. The step $\Delta\tau_{FD} = 0.01$ satisfies this restriction for the conditions studied here and was used throughout.

Setting $q''_2/q''_1 = 0$ in equation (25c) results in the same surface condition as studied by Sammakia *et al.* [6]. However, the present formulation envisions computations for any finite $q''_2/q''_1$. All computations throughout the transient were also made with $q''_2/q''_1 = 0$ for the $Q^*$ values in ref. [6]. These results were in excellent agreement with the earlier results. Then, calculations for $q''_2/q''_1 > 0$ were made. The results are discussed next.

### 3.2. *Numerical results with negligible thermal capacity, i.e.* $Q^* = 0$ *for* $q''_2/q''_1 > 0$

Velocity and temperature responses in water are shown in Figs. 6 and 7 for $q''_2/q''_1 = 5$, and in Figs. 8 and 9 for 0.5. These responses are plotted in terms of $\Delta U$ and $\Delta T$, the changes from the initial steady velocity and temperature profiles, $U_1$ and $T_1$. Thus, only the transient changes are seen. Also shown are both the short-time responses and the eventual steady laminar boundary layer calculations.

The short-time solutions were transformed into the present variables by

$$U - U_1 = \Delta U = \frac{8\tau_{FD}^{3/2}}{\sqrt{Pr(Pr-1)}}(q''_2/q''_1 - 1) \times [i^3(Y\sqrt{Pr}/2\sqrt{\tau_{FD}} - i^3(Y/2\sqrt{\tau_{FD}})] \quad (27)$$

$$T - T_1 = \Delta T = 2\frac{\sqrt{\tau_{FD}}}{\sqrt{Pr}}(q''_2/q''_1 - 1) \times i\,\mathrm{erfc}[Y\sqrt{Pr}/2\sqrt{\tau_{FD}}]. \quad (28)$$

Also, the eventual steady-state quantities are related to values at $\tau_{FD} = 0$ as follows:

$$U_2/U_1 = R^{0.4} f'_0(\eta R^{1/5})/f'_0(\eta) \quad (29a)$$

$$T_2/T_1 = R^{0.8}\phi_0(\eta R^{1/5})/\phi_0(\eta) \quad (29b)$$

where $R = q''_2/q''_1$ and $\eta = Y/(5X)^{0.2}$.

In Fig. 6, for $\tau_{FD} = 2$ and 4, the numerical results for velocity are seen to be in very good agreement with the short-time solution. For $\tau_{FD} = 8$, they lag seriously, as convective momentum effects become important. Steady state arises at about $\tau_{FD} = 25$. Thereafter, there is very little further change. By $\tau_{FD} = 35$, the numerical results are in good agreement with the steady boundary layer calculation.

The associated temperature development profiles are seen in Fig. 7. The numerical and short-time results agree well for $\tau_{FD} = 2$, 4 and 8. The thermal layer is well within the velocity layer. Even though the velocity has departed from the one-dimensional form at $\tau_{FD} = 8$, the temperature response still follows the short-time result. Convective effects have become important by $\tau_{FD} = 15$. Steady conditions are indicated for $\tau_{FD} \geqslant 25$, as again seen from the good agreement with the steady boundary layer calculation.

Figures 8 and 9 are a similar comparison, for a

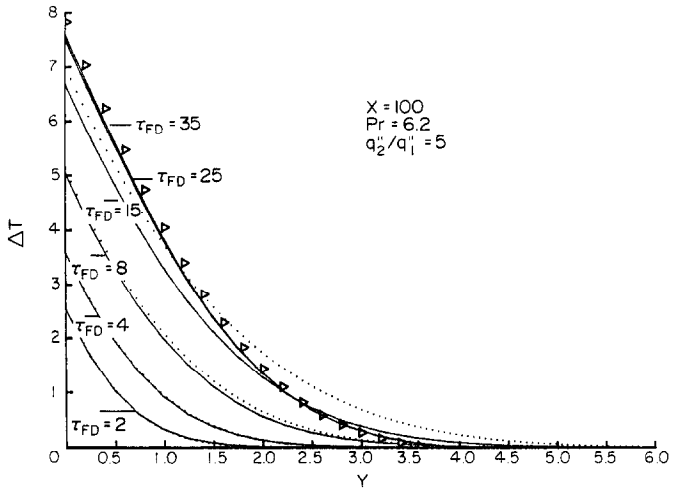


FIG. 7. Incremental temperature profiles across the fluid at various times for $q_2''/q_1'' = 5$ and $Pr = 6.2$: ———, finite-difference calculations; · · · · · · · , short-time analysis; ▷, steady laminar similarity solution.

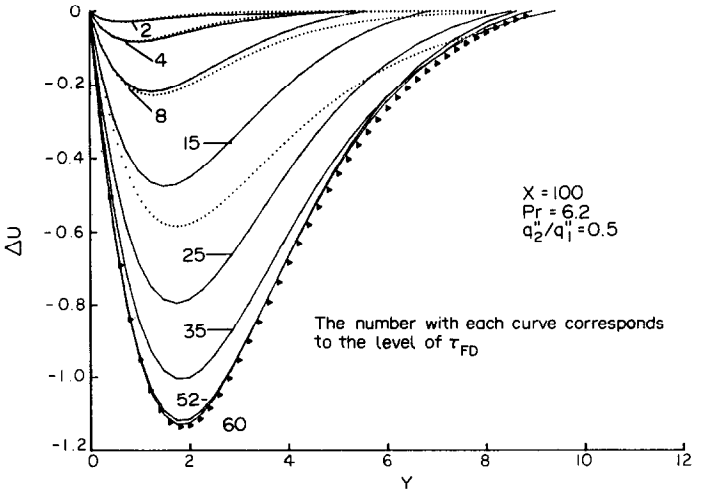


FIG. 8. Incremental vertical velocity profiles across the fluid at various times for $q_2''/q_1'' = 0.5$ and $Pr = 6.2$: ———, finite-difference calculations; · · · · · · · , short-time analysis; ▷, steady laminar similarity solution.

decrease in heating rate, for $q_2''/q_1'' = 0.5$. The numerical velocity results in Fig. 8 are again in good agreement with the short-time predictions for $\tau_{FD} = 2$ and 4. Convective momentum effects then reduce the velocity response below the one-dimensional solution, as seen at $\tau_{FD} = 8$ for $Y > 1.5$. This effect has become much larger at $\tau_{FD} = 15$. Steady flow is achieved at about $\tau_{FD} = 60$. The temperature results in Fig. 9 show similar trends. As in Fig. 7, the agreement with the short-time transport persists to a longer time, for $\tau_{FD} \leqslant 8$.

A comparison of Figs. 6 and 7 with Figs. 8 and 9 shows, as expected, that a decrease in the surface heating level results in a much slower transient. Steady conditions are achieved for $q_2''/q_1'' = 5$ for $\tau_{FD} \approx 25$ and for $q_2''/q_1'' = 0.5$ at $\tau_{FD} \simeq 52$. As seen later, in Section 4, steady state arises at a given downstream location $x$, sometime after the leading edge effect has passed. Increasing the surface heat flux increases the flow velocity. Decreasing it, decreases velocities. This slows the leading edge propagation rate and extends the transient time.

## 4. COMPARISON WITH EXPERIMENTS

Transient flows were generated in water adjacent to a vertical $1.24 \times 0.35$ m surface, consisting of two 0.038 mm foils of Inconel 600, separated by layers of resin impregnated fabric. The assembly was fused at high temperature and pressure. The final composite thickness was 0.28 mm, or 11 mils, and the value of $c''$ was about 440 J m$^{-2}$ K$^{-1}$.

Experiments were carried out in a $1.83 \times 0.62 \times 1.83$ m high stainless steel tank, with glass windows for flow visualization. The initial steady natural convection flow was generated by passing a steady electric

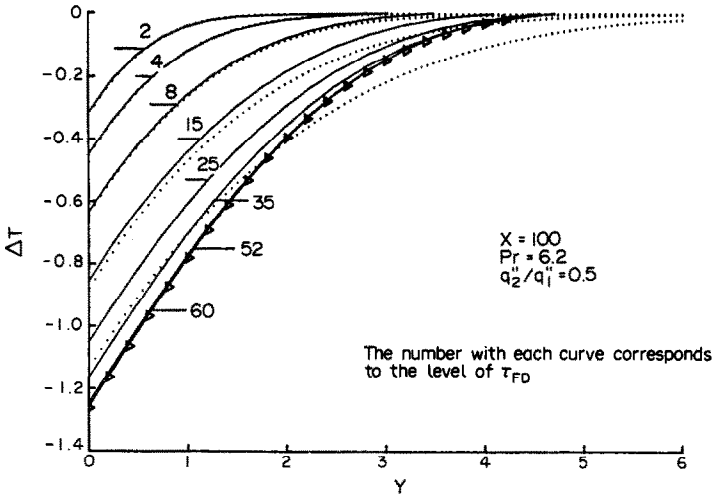


FIG. 9. Incremental temperature profiles across the fluid at various times for $q''_2/q''_1 = 0.5$ and $Pr = 6.2$: ———, finite-difference calculations; · · · · · · ·, short-time analysis; ▷, steady laminar similarity solution.

current through the Inconel surface foils on each side of the assembly. The surrounding water had been deionized to a resistivity level of approximately 1 MΩ cm, to avoid electrical leakage.

Local temperature measurements in the fluid were made using a 0.087 mm diameter copper–constantan thermocouple probe. Surface temperatures were also measured, from thermocouples embedded within the layers of fabric inside the composite surface. All thermocouples were referenced to a water–ice bath. Local velocities were measured with a calibrated DISA 55R14 hot-film probe. Data were digitized, by an automatic data-acquisition system, and stored on magnetic tapes. Flow visualization was of suspended neutrally buoyant particles in the water, illuminated by a plane of He–Ne laser light.

The transient was started by manually abruptly changing the power input to the test surface at a given time. The quality of this step was monitored on the data acquisition system. The power supply response time was typically of the order of a few tenths of a second. This is much faster than the total transient times in this study, typically 40–100 s.

The 12 experimental conditions are listed in Table 1. Transient flow visualizations, local sensor and surface temperature response measurements were taken for each experiment. Transient flow visualization sequences are given first. The transport mechanisms detected, thereby, are later substantiated in terms of local sensor data.

### 4.1. *Flow visualizations*

4.1.1. *Increased heating rate.* Figure 10 is a transient flow response sequence for a sudden heat flux increase, $q''_2/q''_1 = 2.07$. The visualization shows developing flow adjacent to the surface, from the leading edge, downstream to $x = 75$ cm. The surface is on the right-hand side. The symmetric flow on the other side of the composite surface is not shown. All pictures were taken at a small horizontal angle to the surface, to show the complete flow field.

The response in Fig. 10, to an increase in flux, remains a largely laminar boundary region flow, for short times. See Fig. 10(a) at about 42 s. In Fig. 10(b), disturbances have appeared, at the location of the arrow. These amplify as they are convected downstream, in Figs. 10(c) and (d). At $\bar{\tau} = 93$ s, the flow appears turbulent near the arrow, in Fig. 10(e). Later, in Figs. 10(f) and (g), the turbulent flow is progressively swept downstream, out of the field. The flow has partially relaminarized in the final steady state, in Fig. 10(h).

These visualizations show that, initially, no changes arise, either in the flow or in the ambient entrainment patterns, up the entire surface. This response is, therefore, consistent with the laminar model in Section 2. A one-dimensional transient is confined within a thin layer adjacent to the surface. Later, for $x < 50$ cm, the flow remains laminar at all times to the final steady state. However, downstream, the flow became turbulent. It partially relaminarized later, in achieving steady state.

4.1.2. *Decreased heating rate.* The visualization sequence following a decrease in surface heating, $q''_2/q''_1 = 0.106$, is seen in Fig. 11. In Fig. 11(a), at 47 s, again no disturbances are seen. In Fig. 11(b), there is a small outer region of disturbances at about mid-height. These have collectively become a counter-clockwise vortex, while being convected downstream, in Fig. 11(c). The center of the vortex is seen to be near the outer edge of the velocity layer. A second vortex, trailing the first one, is first seen in Fig. 11(d). In Fig. 11(e), the flow within the higher vortex appears to be turbulent. In Fig. 11(f), this vortex is now near the top of the photograph and the flow in the lower vortex also appears turbulent. Both are convected

Table 1. Experimental conditions for data in Section 4

| Run | $q_1''$ (W m$^{-2}$) | $q_2''/q_1''$ | $x$ (cm) | $Q^*$ | $E_1$ | $E_2$ | $(u_1-u_{1_{BL}})/u_{1_{BL}}$ | $(t_1-t_{1_{BL}})/t_{1_{BL}}$ | Type of experiment |
|---|---|---|---|---|---|---|---|---|---|
| 1 | 279 | 2.07 | 0–75 | 0.71 | 15.9† | 18.1† | — | — | Flow visualization |
| 2 | 574 | 0.11 | 0–75 | 0.85 | 18.5† | 11.7† | — | — | |
| 3 | 90 | 11.30 | 29 | 0.54 | 8.3 | 13.5 | 0.07 | 0.07 | Local sensor measurements |
| 4 | 588 | 3.01 | 29 | 0.86 | 12.3 | 15.4 | 0.01 | 0.05 | |
| 5 | 588 | 0.15 | 29 | 0.86 | 12.1 | 8.3 | 0.03 | 0.01 | |
| 6 | 1017 | 0.28 | 29 | 0.99 | 13.7 | 10.5 | 0.06 | 0.02 | |
| 7 | 53 | 16.64 | 49 | 0.48 | 9.2 | 16.2 | 0.04 | 0.01 | |
| 8 | 589 | 2.31 | 49 | 0.86 | 15.0 | 17.7 | 0.07 | 0.02 | |
| 9 | 589 | 0.09 | 49 | 0.87 | 14.9 | 9.3 | 0.07 | 0.04 | |
| 10 | 1143 | 0.13 | 49 | 1.02 | 17.1 | 11.4 | 0.15 | 0.14 | |
| 11 | 82 | 5.61 | 32.6, 43.6, 96.8 | 0.52 | 13.5‡ | 19.1‡ | — | 0.02, 0.05, 0 | Surface temperature measurements |
| 12 | 956 | 0.34 | 32.6, 43.6, 96.8 | 0.96 | 22.4‡ | 17.8‡ | — | 0.02, 0.05, 0.02 | |

† Evaluated at $x = 75$ cm.
‡ Evaluated at $x = 96.8$ cm.

downstream in Fig. 11(g). Laminar conditions are restored locally with their passage. The eventual steady flow, in Fig. 11(h), is completely laminar, for the relatively low flux $q_2'' = 61$ W m$^{-2}$.

This response shows many similarities with that of Fig. 10. Near the leading edge, the flow is always laminar. Downstream, transient transition occurs. Laminar conditions are later restored. However, the orderly vortex pattern in Fig. 11 is an entirely different effect. It was seen only for large decreases in surface heating, that is, for small $q_2''/q_1'' < 1$. Runs with $q_2''/q_1''$ near 1.0 did not generate such well-defined vortices. Their disturbance patterns were instead similar to those with $q_2''/q_1'' > 1.0$.

4.2. *Local sensor measurements*

Transient local velocity and temperature measurements were also made for the flux conditions and locations listed in Table 1. Typical data are presented in Figs. 12–14, for downstream locations $x = 0.29$ and 0.49 m, for several transients. Some of these measurements were in flows which remained laminar during the transient. Some were in flows which are in transition; either in the beginning, during or near the end of the transient.

4.2.1. *Responses upstream.* Measured velocity and temperature responses are seen in Figs. 12 and 13 for $q_2''/q_1'' = 11.30$, 3.01, 0.15 and 0.28, as curves (a)–(d). In Fig. 12 the velocity sensor was at $x = 0.29$ m and

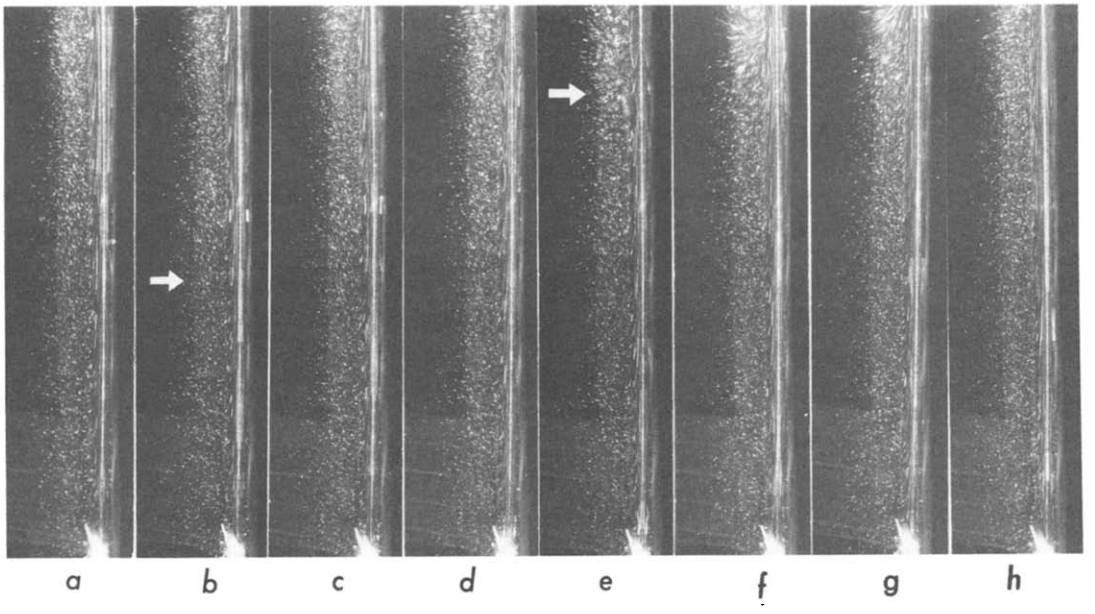


FIG. 10. Flow visualization in water following an increase in surface heating from $q_1'' = 279$ W m$^{-2}$ to $q_2'' = 547$ W m$^{-2}$ for $0 < x < 75$ cm. Exposure durations in seconds are (a) 34–42, (b) 59.5–67.5, (c) 68–76, (d) 76.5–84.5, (e) 85–93, (f) 102–110, (g) 110.5–118.5 and (h) 144.5–152.5.

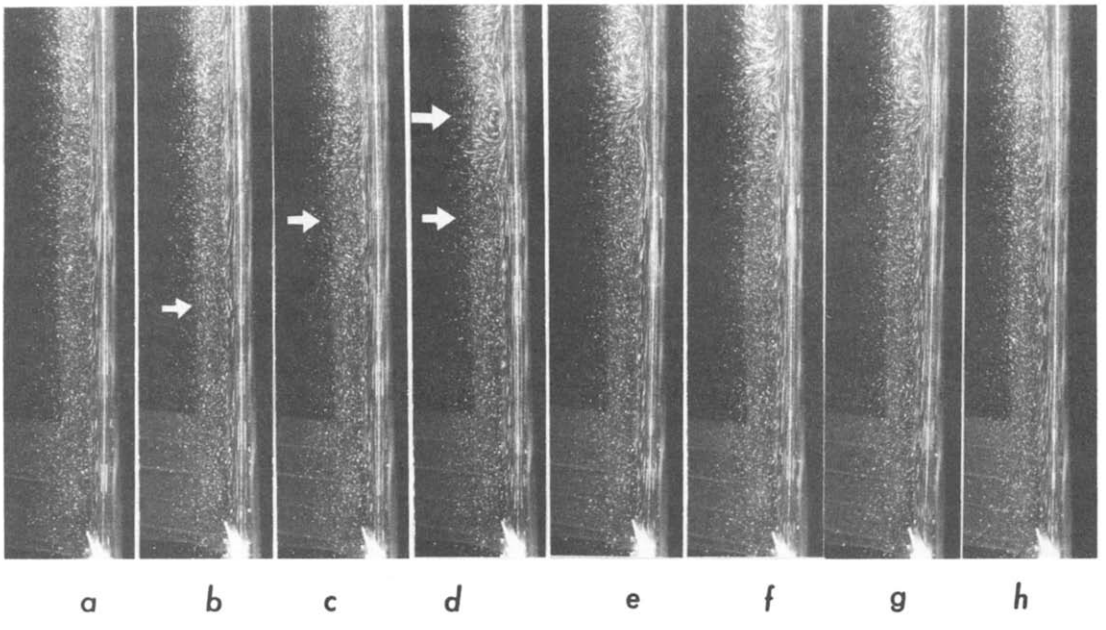


FIG. 11. Flow visualization in water following a decrease in surface heating from $q_1'' = 574$ W m$^{-2}$ to $q_2'' = 61$ W m$^{-2}$ for $0 < x < 75$ cm. Exposure durations in seconds are (a) 42–52, (b) 94.5–104.5, (c) 115.5–125.5, (d) 136.5–146.5, (e) 147–157, (f) 157.5–167.5, (g) 168–178 and (h) 346.5–356.5.

$y = 2.21$ mm. This is close to the location of the velocity maximum of the initial steady flow for $q_1'' = 588$ W m$^{-2}$. The corresponding temperature responses for the same heating conditions, are in Fig. 13, but at $x = 0.29$ m and $y = 1.68$ mm. Again the incremental responses of the physical velocity, $\Delta u$, and temperature, $\Delta t$, are shown, to emphasize the changes during the developing transient.

The differences between the initial steady sensor data and the corresponding laminar similarity profiles are listed in Table 1, in the last two columns. Figures 12 and 13 show both the calculated short-time response, from Section 2, and the complete response from the numerical calculations, from Section 3. Surface thermal capacity was included in the numerical calculations. Computed values of $Q^*$ for each test are also listed in Table 1.

The heating transient in Fig. 12, for $q_2''/q_1'' = 11.30$ starts from a steady flow generated by a very low flux level. A large increase follows. Since the thermal capacity parameter is $Q^* = 0.54$, its effect on response is small. Both the short-time and finite-difference results are in close agreement with the measured response for the first 20 s. Later, as the changing thermal effect penetrates further out, the sensor response lags the short-time solution. The numerical results

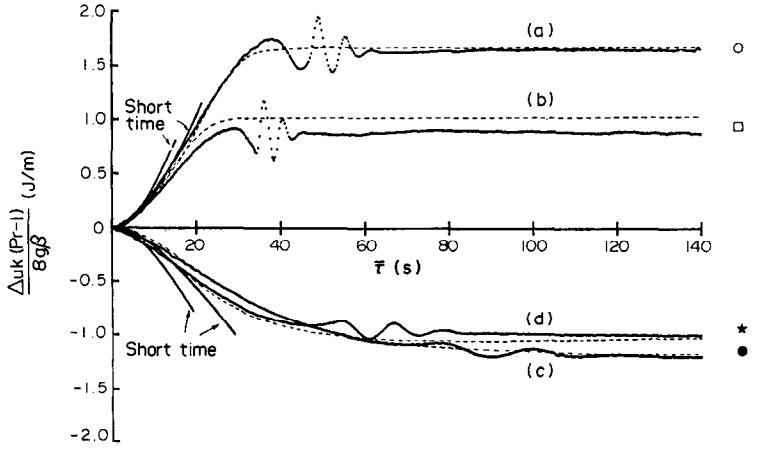


FIG. 12. Fluid velocity response following a change in surface heating at $x = 0.29$ m and $y = 2.21$ mm. (a) $q_1'' = 90$ W m$^{-2}$, $q_2'' = 1017$ W m$^{-2}$, (b) $q_1'' = 588$ W m$^{-2}$, $q_2'' = 1768$ W m$^{-2}$, (c) $q_1'' = 588$ W m$^{-2}$, $q_2'' = 90$ W m$^{-2}$ and (d) $q_1'' = 1017$ W m$^{-2}$, $q_2'' = 284$ W m$^{-2}$, ———, short-time analysis; · · · · · · ·, data; and – – – – –, finite-difference calculations. Symbols on the right-hand side correspond to steady similarity solution for $Pr = 6.2$.

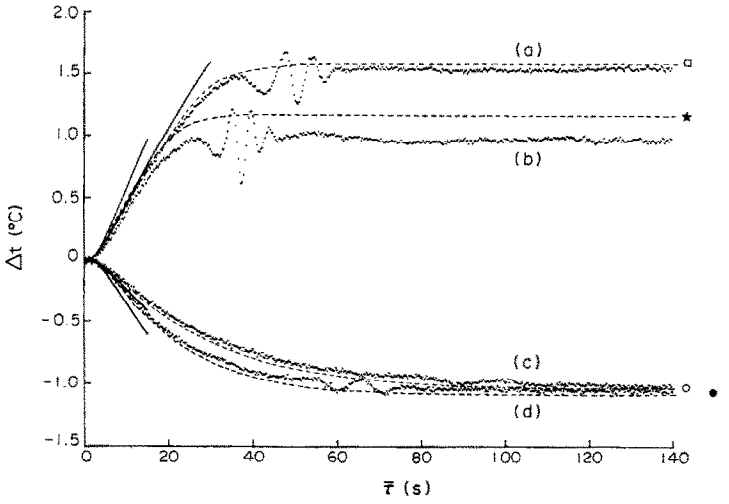


FIG. 13. Fluid temperature responses following a change in surface heating at $x = 0.29$ m and $y = 1.68$ mm. Conditions (a)–(d) are the same as in Fig. 12.

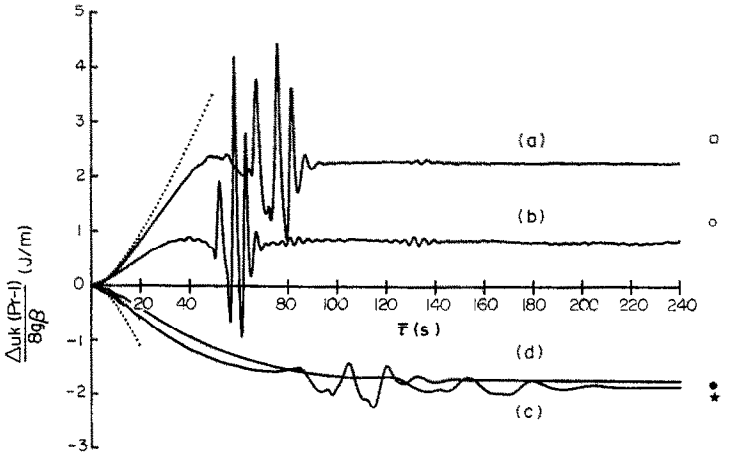


FIG. 14. Fluid velocity response following a change in surface heating at $x = 0.49$ m and $y = 2.21$ mm. (a) $q_1'' = 53$ W m$^{-2}$, $q_2'' = 882$ W m$^{-2}$, (b) $q_1'' = 589$ W m$^{-2}$, $q_2'' = 1363$ W m$^{-2}$, (c) $q_1'' = 589$ W m$^{-2}$, $q_2'' = 53$ W m$^{-2}$ and (d) $q_1'' = 1143$ W m$^{-2}$, $q_2'' = 153$ W m$^{-2}$. · · · · · ·, short-time analysis; ———, data. Symbols on the right-hand side correspond to steady similarity solution for $Pr = 6.2$.

remain in closer agreement. At $\bar{\tau} \simeq 40$ s, the sinusoidal variation in both $\Delta u$ and $\Delta t$ mark the passage of the leading edge effect. These disturbances decay very quickly. The data show steady state at about $\bar{\tau} \simeq 70$ s. The eventual measured steady velocity and temperature levels are in good agreement both with the calculated similarity solution, shown as symbols on the right, and with the finite-difference calculations, converged to steady state, and shown as asymptotes.

The heating transient in Fig. 12(b) starts from a higher initial flux level, $q_1'' = 588$ W m$^{-2}$, run 4 in Table 1. The input flux was then changed to 1768 W m$^{-2}$, the maximum level studied in these measurements. Transient response data agree with the finite-difference prediction for the first 10 s. Thereafter, the sensor response lags the numerical results. A periodic disturbance, as before, arises earlier, at $\bar{\tau} \simeq 30$ s. Steady conditions are reached at $\bar{\tau} \simeq 50$ s, and both velocity and temperature data are below the laminar calculation, since this is a region of transition.

The downstream transition of a steady vertical natural convection flow in water was measured in detail in ref. [8]. The beginning of velocity transition was found to be reliably signalled by a decrease in velocity level near the laminar maximum. On the other hand, thermal transition caused steepening of the temperature profile from the laminar trend, close to the surface. These measurements indicated that steady transition began at a fixed value of the parameter $E = G^*(\nu^2/gx^3)^{2/15}$. Velocity and later thermal transition were characterized by $E = 13.6$ and 15.2, respectively. The values $E_1$ and $E_2$ in Table 1 are the estimated values of $E$ based on $q_1''$ and $q_2''$, respectively, for the present experiments.

Curves (c) and (d) in Figs. 12 and 13 show the transient following a decrease in heating. The data follow the short-time analysis for $\bar{\tau} \leqslant 10$ s. Later, as convective effects develop, they agree with numerical computations. The periodic disturbances seen before steady state are smaller in amplitude than for increased heating, in curves (a) and (b). The final steady transport is laminar and the data agree well with similarity solution.

4.2.2. *Responses further downstream.* Transient velocity responses further downstream at $x = 0.49$ m, are shown in Fig. 14, for conditions 7–10 in Table 1. The temperature response is not shown. The $q''_2/q''_1$ values are close to those for the upstream measurements shown in Figs. 12 and 13. Since exact control of power input was not possible, there is some difference in input flux. Responses (a) and (b) are for increases and (c) and (d) are for decreases. Only the short-time transient solution and laminar similarity results are shown in Fig. 14. No numerical calculations were made for these conditions, since they are beyond the beginning of velocity transition, either initially or in the final developed flow.

The short-time response in Fig. 14(b) is initially similar to that for heating conditions in Fig. 12. The response in Fig. 14(a) agrees better with the short-time solution than Fig. 14(b), since $q''_1$ is less. A higher flux results in a greater initial thickness of the thermal boundary layer. The initial transient effects then remain confined within this layer for a longer time. Since the steady flow is in transition, the resulting final velocity levels are below the laminar calculation. Just before the final flow condition is achieved, large periodic disturbances pass by, as also seen upstream in Figs. 12 and 13.

Responses following a reduction in heating are seen in Figs. 14(c) and (d). They agree with the short-time solution to about $\bar{\tau} \leqslant 10$ s. The periodic disturbances are again smaller in amplitude than for $q''_2/q''_1 > 1$ as in Figs. 14(a) and (b). Table 1 indicates that the initial flow, corresponding to $q''_1$, is in transition, for both conditions, Figs. 14(c) and (d). This led to initial velocity levels below the laminar theory. Recall that the incremental velocity data in Fig. 14 are obtained by subtracting the initial measured levels. Therefore, the steady mean levels in Figs. 14(c) and (d) are above the laminar predictions.

4.3. *Measured temperature response of the heating surface*

The response of the thermocouples embedded in the surface, at $x = 32.6$, 43.6 and 96.8 cm are shown in Fig. 15. The upper curves, Fig. 15(a), are for run 11, $q''_2/q''_1 = 5.61$. The lower curves, Fig. 15(b), are for run 12, $q''_2/q''_1 = 0.34$. Also shown in Fig. 15 are both the short-time solutions and numerical results at $x = 32.6$ and 43.6 cm. Computations were not made for $x = 96.8$ cm, since this flow was not laminar.

For Fig. 15(a), the surface temperature initially rises in agreement with the one-dimensional prediction at all three locations. Steady conditions are achieved at about $\bar{\tau} = 40$ s at $x = 32.6$ cm and slightly later at $x = 43.6$ cm. Only small disturbances arise, before steady state. At $x = 96.8$ cm, however, the surface temperature decreases below the steady-state asymptote, during the 110–160 s interval. It then recovers to the final steady state.

A similar effect was seen in ref. [3] in heating transients started from quiescence. The transient flow far downstream of the leading edge becomes turbulent. The resultant large-scale turbulent transport improves heat transfer, causing a large drop in the surface temperature. This effect is then swept downstream. The surface temperature increases as the flow partially relaminarizes. Finally, the eventual temperature levels are in good agreement with the similarity solutions, even though the values of $E_1$ and $E_2$ at $x = 96.8$ cm are larger than at the beginning of transition. The same trend was also reported in ref. [9]. This is because surface thermal capacity effects damp out smaller flow temperature disturbances. Measured surface temperature levels agree with the laminar trend, for $E$ levels significantly beyond the first detection of transition by the local sensors in the fluid.

The response for decreased surface heating, Fig. 15(b), shows similar trends. There is initial agreement with the short-time solution at all three $x$ locations. Steady conditions at $x = 32.6$ and 43.6 cm are close to the laminar predictions. The surface temperature at $x = 96.8$ cm is lower during the interval 100–170 s. This is again caused by transition during the transient. Later, relaminarization occurs and the surface temperature increases. The temperature response in Fig. 15 shows that both an increase and a decrease in the surface flux causes transient transition, sufficiently far downstream. This is a heat transfer enhancement mechanism during a large part of the transient.

## 5. CONCLUSIONS

Transient convection response, due to a change in surface heating rate, has been determined for a wide range of conditions. The short-time response is purely diffusive and is confined within the initially established boundary region. Later, convective effects modify the changing velocity and temperature levels and distributions. Before steady conditions are again achieved, periodic disturbances propagate downstream, from the leading edge. Their amplitude increases and they cause downstream transient transition to turbulence.

As a result, a large temporary increase in heat transfer effectiveness occurs. This is seen as a decrease in the surface temperature. This occurs both for $q''_2/q''_1 > 1$ and $q''_2/q''_1 < 1$. This suggests the possibility of modulating heating rates around their mean level, to increase heat transfer performance. By properly adjusting the modulation pattern, the turbulent flow arising during the transient may become continuous.

Increasing disturbance levels downstream strongly

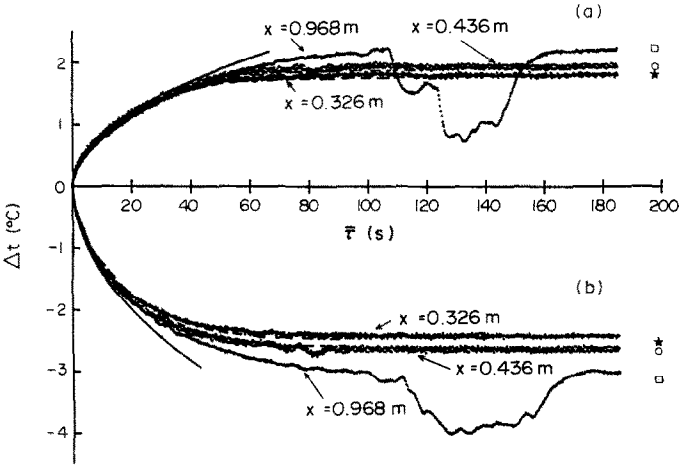


FIG. 15. Surface temperature response following a change in surface heating for various $x$. (a) $q_1'' = 82$ W m$^{-2}$, $q_2'' = 460$ W m$^{-2}$ and (b) $q_1'' = 960$ W m$^{-2}$, $q_2'' = 323$ W m$^{-2}$, ———, short-time analysis; · · · · · · ·, data; and – – – –, finite-difference computations for $Pr = 6.2$. Symbols on the right-hand side are steady laminar boundary layer predictions.

imply transient instability. The analysis of such instability will be very complicated, since both the base flow and the disturbances are changing in time. Past approaches to assess the stability of such flows are summarized in ref. [3]. The disturbance data obtained in this study may serve as a guide in such modelling efforts.

*Acknowledgements*—The authors acknowledge support for these measurements and their interpretation under NSF Grants MEAM 82-17756 and CBT 84-18517. Y. Joshi was partially supported by the Naval Postgraduate School Research Foundation during the preparation of the final manuscript.

## REFERENCES

1. C. R. Illingworth, Unsteady laminar flow of gas near an infinite plate, *Proc. Camb. Phil. Soc.* **46**(4), 603–613 (1950).
2. Y. Joshi, Transient natural convection flows and natural convection flows in porous media, Ph.D. Dissertation, University of Pennsylvania (1984).
3. Y. Joshi and B. Gebhart, Transition of transient vertical natural convection flow in water, *J. Fluid Mech.* **179,** 407 (1987).
4. D. B. Ingham, Flow past a suddenly cooled vertical plate, *J. Inst. Math. Applic.* **22,** 189 (1978).
5. D. B. Ingham, J. H. Merkin and I. Pop, Flow past a suddenly cooled vertical flat surface in a saturated porous medium, *Int. J. Heat Mass Transfer* **25,** 1916 (1982).
6. B. Sammakia, B. Gebhart and Z. H. Qureshi, Measurements and calculations of transient natural convection in water, *J. Heat Transfer* **104,** 644 (1982).
7. B. Carnahan, H. A. Luther and J. O. Wilks, *Applied Numerical Methods*, pp. 474–481. Wiley, New York (1969).
8. Y. Jaluria and B. Gebhart, On transition mechanisms in vertical natural convection flow, *J. Fluid Mech.* **66,** 309 (1974).
9. Z. H. Qureshi and B. Gebhart, Transition and transport in a buoyancy driven flow in water adjacent to a vertical uniform flux surface, *Int. J. Heat Mass Transfer* **21,** 1967 (1978).

## APPENDIX. ESTIMATION OF THE RELATIVE SURFACE THERMAL CAPACITY EFFECT

A change in surface heating rate from $q_1''$ to $q_2''$ initially results in one-dimensional incremental transport. Closed form solutions for such transport were obtained for $Q^* = 0$. Here we examine the conditions under which this is a reasonable approximation. The surface thermal capacity may be neglected, compared to that of the fluid, when

$$(\rho_s c_{ps} W/2) \ll \delta_t(\bar{\tau}) c_{pf} \rho_f. \tag{A1}$$

In inequality (A1), $W$ is the thickness of the surface element and $\delta_t(\bar{\tau})$ is the thickness of the thermal layer. The upper bound on $\delta_t(\bar{\tau})$ is the layer thickness for $Q^* = 0$. In non-dimensional form this is $\delta_t/(4\alpha\bar{\tau})^{1/2} \simeq 2$. Assume that if the left-hand side in inequality (A1) does not exceed 5% of the right-hand side, the surface thermal capacity may be taken as negligible. Then

$$\bar{\tau} \geqslant (\rho_s c_{ps} W/\rho_f c_{pf})^2/(0.16\alpha). \tag{A2}$$

For the present experiments, $(\rho_s c_{ps} W) = 883$ J m$^{-3}$. Substituting fluid properties at 300 K we get

$$\text{for water} \quad \bar{\tau} > 1.19 \text{ s}$$

$$\text{for air} \quad \bar{\tau} > 1.57 \times 10^5 \text{ s}.$$

Thus, for water, the surface thermal capacity effect becomes small very quickly. In air, this effect is very large. An extremely thin surface would be required for the surface thermal capacity effect to be negligible in air.

## REPONSE TRANSITOIRE D'UN ECOULEMENT PERMANENT VERTICAL SOUMIS A UN CHANGEMENT DE CHAUFFAGE A LA SURFACE

**Résumé**—La réponse transitoire de convection naturelle, à la suite d'un changement du flux de chauffage à la surface, a été mesurée pour un domaine de chauffage de l'eau. Un nouvel état permanent est atteint au travers de plusieurs mécanismes distincts. Le premier est un transitoire purement diffusif près de la surface qui s'accorde avec la solution donnée. Ensuite, apparait un transitoire général qui se développe. Les solutions de l'écoulement indiquent un effet de bord d'attaque se propageant vers l'aval. Puis le transitoire s'approche d'un autre écoulement permanent. Les visualisations et les mesures locales de vitesse et de température s'accordent aussi avec les calculs. Les écoulements en amont demeurent laminaires pendant le transitoire. En aval, la transition et la turbulence variables augmentent le transfert local de chaleur. Ceci suggère que l'accroissement général de transfert thermique peut être atteint par des changements programmés des niveaux de flux de chaleur imposés.

## ÜBERGANGSVERHALTEN EINER STATIONÄREN VERTIKALEN STRÖMUNG BEI EINER VERÄNDERUNG DER WANDWÄRMESTROMDICHTE

**Zusammenfassung**—Das Übergangsverhalten einer natürlichen Konvektionsströmung bei einer Änderung der Wandwärmestromdichte wurde für eine Reihe von Heizbedingungen für Wasser gemessen. Ein neuer stationärer Zustand stellt sich nach Durchlaufen verschiedener Prozesse ein. Der erste ist eine rein diffusionsbedingte Veränderung nahe der Wandoberfläche—dies wird durch die angegebenen Gleichungen gut beschrieben. Von hier breitet sich die Störung stromabwärts aus. Das Übergangsverhalten der Transportvorgänge, welches durch Strömungsbeobachtung und durch Messung von örtlicher Geschwindigkeit und Temperatur ermittelt wird, stimmt ebenfalls mit den Berechnungen überein. Stromaufwärts bleibt die Strömung während des gesamten Vorganges laminar. Stromabwärts erhöht sich der örtliche Wärmeübergang durch die instationären Vorgänge und durch Turbulenz. Dies legt die Idee nahe, daß durch bewußt vorgenommene Änderungen der Wärmestromdichte der Wärmeübergang ganz allgemein verbessert werden kann.

## ВЛИЯНИЕ ИЗМЕНЕНИЯ ИНТЕНСИВНОСТИ НАГРЕВА ТВЕРДОЙ ПОВЕРХНОСТИ НА ГИДРОДИНАМИКУ СТАЦИОНАРНОГО ВЕРТИКАЛЬНОГО ПОТОКА

**Аннотация**—При различных условиях нагрева найдено влияние изменения интенсивности нагрева твердой поверхности на режим естественной конвекции в объеме воды. Показано, что новое стационарное состояние достигалось в результате определенной последовательности гидродинамических процессов. Вначале у поверхности возникает чисто диффузионный перенос, что согласуется с полученными решениями. Затем нестационарное состояние распространяется на всю область вниз по течению. В этом случае решения указывают на влияние передней кромки, которое распространяется вниз по течению. После этого отмечается приближение к новому стационарному состоянию. Нарушение стационарности течения, наблюдаемое визуально и определяемое измерениями локальной скорости и температуры, также согласуется с расчетами. В течение всего переходного процесса поток вверх по течению остается ламинарным. Вниз по течению как переходный процесс, так и турбулентность усиливают местный перенос тепла. Это свидетельствует о том, что процесс теплообмена можно интенсифицировать, если определенным образом изменять величину подводимого теплового потока.